ARCHIVE OF MECHANICAL ENGINEERING

DOI: 10.24425/ame.2022.140410 2022, Vol. 69, No. 1, pp. 77–98

Mohamed Lamine BENLEKKAM [1,2], Driss NEHARI [3]

Hybrid nano improved phase change material for latent thermal energy storage system: Numerical study

Received 9 July 2021, **Revised** 14 November 2021, **Accepted** 24 November 2021, **Published online** 21 January 2022

Keywords: phase change material (PCM) latent heat storage, melting and solidification, thermal energy storage, hybrid nano-particles, LHTESS

The phase change materials (PCM) are widely used in several applications, especially in the latent heat thermal energy storage system (LHTESS). Due to the very low thermal conductivity of PCMs. A small mass fraction of hybrid nanoparticles TiO_2–CuO (50%–50%) is dispersed in PCM with five mass concentrations of 0%, 0.25%, 0.5%, 0.75% and 1 mass % to improve its thermal conductivity. This article is focused on thermal performance of the hybrid nano-PCM (HNPCM) used for the LHTESS. A numerical model based on the enthalpy-porosity technique is developed to solve the Navier-Stocks and energy equations. The computations were conducted for the melting and solidification processes of the HNPCM in a shell and tube latent heat storage (LHS). The developed numerical model was validated successfully with experimental data from the literature. The results showed that the dispersed hybrid nanoparticles improved the effective thermal conductivity and density of the HNPCM. Accordingly, when the mass fraction of a HNPCM increases by 0.25%, 0.5%, 0.75% and 1 mass %, the average charging time improves by 12.04 %, 19.9 %, 23.55%, and 27.33 %, respectively. Besides, the stored energy is reduced by 0.83%, 1.67%, 2.83% and 3.88%, respectively. Moreover, the discharging time was shortened by 18.47%, 26.91%, 27.71%, and 30.52%, respectively.

1. Introduction

During the last years, climate change and the increase of greenhouse gas emissions became the concern of the world's governments. This problem encouraged them to look for better alternatives, i.e., switch to renewable energies and use them

✉ Mohamed Lamine BENLEKKAM, e-mail: mohamed_benlekkam@yahoo.fr

[1]Department of Science and Technology, University of Tissemsilt, Tissemsilt, Algeria

[2]Laboratory of Smart Structure, University of Ain Temouchent, Ain Temouchent, Algeria

[3]Laboratory of Hydrology and Applied Environment, University of Ain Temouchent, Algeria

more efficiently. Among the most efficient solutions is the "thermal solar energy". However, its intermittent nature creates an imbalance of required energy needs between day and night. The thermal energy storage (TES) system helps to recover the energy supply and demand balance. There are three types of thermal energy storage: sensible heat, latent heat, and thermochemical heat, among which the latent heat thermal energy storage technique presents a good efficiency. In fact, in the latent heat storage (LHS) a phase change material (PCM) is used to absorb and release thermal energy during its melting and solidification cycles [1]. However, the PCM suffers from its low thermal conductivity (0.1–0.7 W/(m K)), which decreases the thermal performance of TES systems. Hence, several researchers try to develop an improved technique to increase the heat transfer rate inside the PCM, such as application of fins, TES system orientation, and nanoparticles additives [2–4].

Firstly, the fins represent an extended surface through the PCM in the TES system. They present an effective solution due to their ability to improve the heat transfer inside the PCM, which allows a uniform temperature distribution in the TES system. Al-Abidi et al. [5] studied the heat transfer improvement in a triplex tube heat exchanger (TTHX). Their obtained results which showed that the PCM melting time was influenced by the fin's length more than by its thickness, which reduced the melting time by 26.1% and 56.6% for the fin's length of 10 and 42 mm, respectively, compared to the non-finned heat exchanger. Furthermore, Yang et al. [6] studied numerically the effect of annular fins with several numbers, thicknesses, and heights of fins to improve the thermal performance of the TES unit. They noticed that the application of fins can reduce the charging time by 65%. Zhao et al. [7] numerically studied the PCM melting by using fins and different metal foams such as copper, aluminum and nickel. They found that the melting rate of PCM was enhanced by 60%, when using a fixed number and thickness of the fins. Moreover, the fins were more efficient than the metal foams for heat transfer enhancement.

Similarly, the orientation and the tilt angle of the TES unit can also improve its thermal performance by promoting the natural convection inside the molten PCM. Longeon et al. [8] conducted an experimental and numerical investigation of a vertical annular TES unit and the HTF injection side. They found that the natural convection dominated the heat transfer during the melting cycle more than the solidification. Besides, they reported that the HTF injection from the upside was more effective for the charging process, whereas the downside HTF inlet was suitable for the discharging process. Seddegh et al. [9] performed an experimental and numerical study to investigate the performance of cylindrical and conical storage units. Both of the units were oriented vertically. The authors reported that the conical unit stored more energy than the cylindrical one for the same charging time due to the strong natural convection. Moreover, Siyabi et al. [10] conducted an experimental and numerical study on the effect of the TES inclination. They revealed that a system tilted by 45° allows the fastest charging/melting process compared with a horizontal case. Joybari et al. [4] investigated experimentally the

effect of the geometrical enhancement of the heat transfer inside a single- and a multiple-tube vertical LHS unit. They found that both the charging and discharging process were faster by 79% in the multiple-tube unit than the processes in the single-tube one due to the greater heat transfer surface. On the other hand, the turbulent regime of the HTF flow does not affect the melting process.

Despite the significant thermal improvement, the fins increase the net weight of the TES system. Hence, the use of nanoparticles dispersed into the pure PCM can be a better way to improve its thermophysical properties. The solidification process of the Nano-enhanced PCM (NePCM) in a LHS unit has been tested numerically by Sebti et al. [11]. The enthalpy porosity method was used to simulate the phase change transition. The authors found that the use of copper dispersed nanoparticles increased thermal conductivity and the conductive heat transfer rate, thus reducing the total time for the complete solidification. Dhaidan et al. [12] presented an experimental and a numerical investigation of the NePCM inside a cross-section of two concentric cylinders. They reported that the inclusion of nanoparticles accelerated the melting time by increasing the PCM's effective thermal conductivity for low concentration. However, the high quantities of nanoparticles make it longer due to the increase of nanoparticles agglomeration and viscosity effects. The authors recommended using an eccentric configuration geometry by lowering the center of the internal cylinder to increase the surface area and the amount of the NePCM exposed to the buoyancy-driven convective flow effect. Ren et al. [13] compared the effect of nanoparticles and metal foam on a LHS system. Different concentrations of nano-additives, metal foam porosity, heat pipe radius, and pore size were numerically analyzed by using the enthalpy-based immersed boundary lattice Boltzmann method. They found that the nanoparticles, the metal foam, the larger heat pipe radius and the pore size can improve the melting process, whereas the storage capacity decreases. However, optimal values of nano-additives and metal foam porosity can provide better energy storage performance. In addition, a lower pore size affects the natural convection which increases the melting time. Nie et al. [14] conducted a parametric study on the charging process for the vertical TES unit. They found that the HTF upside injection was more effective in convection domination, whereas the bottom injection was better for the conduction. Besides, the inclusion of nanoparticles improved the conduction heat and decreased the total energy storage. Based on the enthalpy porosity method, Gorzin et al. [15] investigated numerically the solidification process in a multi-tube heat exchanger (MTHX) for the LHS. They reported that the PCM distribution in inner and outer tubes reduced the solidification time by 62%. Moreover, the increase of CuO nanoparticles fraction from 0% to 4% allowed reducing the solidification time from 62 min to 46 min, i.e., obtaining a 25% improvement. Khatibi et al. [16] investigated a discharging process for three types of nano-enhanced TES units. They carried out a 2D numerical study of PCM incorporating different nanoparticles with several volume fractions. The authors reported that application of nano additives decreases the solidification time,

whereas the CuO with a 4% volume fraction causes that the discharging time decreases. Manoj Kumar et al. [17] investigated the effect of low mass% SiO_2 nanoparticles on the thermal properties of the paraffin wax as the PCM. It was reported that the thermal conductivity of the nano-PCM was significantly improved, whereas its storage capacity decreased. Besides, the inclusion of SiO_2 increased the PCM's time life. Nedjem et al. [2] found through a numerical study that the discharging rate for the nano-PCM based on graphene nanoplatelets (GNPs) decreased with the increment of GNPs, whereas the stored energy decreased. Moreover, the melting time dropped by 9.5% for 1 wt% of GNPs concentration. Furthermore, 3% of nanoplatelets led to an increase in the PCM's viscosity, thus slowing down the liquid PCM, which disabled the domination of natural convection.

Overall, introducing one type of nanoparticle into a PCM can improve its thermophysical properties, then the performance of the TES system. However, the use of two types of nanoparticles has not been widely studied. Recently, Manoy Kumar et al. [18] performed an experimental study on performance enhancement of the TES system for five cases, of which the first was without PCM, the second with a pure PCM, and the last three cases concerned 0.5%, 1.0%, and 2.0% mass fraction of hybrid nanoparticles inside the PCM. The authors obtained a hybrid nano-PCM (HNPCM) by blending 50–50% of SiO_2 and CeO_2 for each mass fraction used. They found that the maximum HNPCM thermal conductivity was improved by 65.56%, with a 2.0% mass fraction. Furthermore, they noticed that the hybrid nanoparticles within PCM provided a synergetic combination, which improved the thermal performance of the system under investigation compared with that applying a single type of nanoparticles, found in the literature. In their recent experimental study, P. Manoy Kumar et al. investigated the effect of using hybrid nanoparticles (SiO_2–CeO_2) inserted into paraffin with 0, 0.5, 1.0, and 2.0 mass fractions on its thermophysical properties. They found that the dispersion of hybrid nanoparticles in the PCM did not affect its chemical structure. Moreover, the relative thermal conductivity and stability of the HNPCM were boosted by 115.49% and 165.56%, respectively. Further, they noticed that the supercooling effect was reduced by more than 35% for 2% of the hybrid nano-additive. Besides, they recommended 1% of hybrid nanoparticles within paraffin for getting a better thermal performance of low-temperature solar thermal systems due to the low change in their thermal storage capacity.

Although various researchers [12, 15, 19, 20] have studied the nano-improvement of a shell and tube LHS system for a single type of nanoparticles, none of them have studied the influence of hybrid nano-PCM (HNPCM). Moreover, an improvement based on a single type of nanoparticle is solely dependent on its thermophysical properties, especially thermal conductivity and viscosity. For the present work, we used the TiO_2 and CuO metal oxide, which has several outstanding properties like stability and chemical inertness. Therefore, the employment of TiO_2–CuO can offer a better improvement.

In this study, we carefully investigated the effect of hybrid nanoparticles on the thermal performance of a shell and tube TES unit. Similar quantity of TiO_2–CuO was dispersed in a paraffin-based PCM with five mass concentrations of 0, 0.25, 0.5, 0.75, and 1 wt%. The present study aims at properly evaluating the effect of hybrid nanoparticles mass concentration on the liquid fraction, the complete-time, the total stored energy, and the total temperature of the HNPCM for both charging (melting) and discharging (solidification) process.

2. Mathematical model

The configuration of the LHS system under investigation, which was studied by Hosseini et al. [21] in their experiment is shown in Fig. 1. This LHS system is composed of a shell and a copper tube heat exchanger. The length, the outer and the inner diameter of the shell and the tube are 1 m, 0.085 m, and 0.022 m, respectively. The exterior of the unit is completely insulated. We kept the same configurations as in [21] in our numerical study. The space between the shell and the tube was filled by a PCM, which was paraffin [22]. A hybrid TiO_2–CuO nanoparticles are dispersed within the PCM for enhancing its thermal properties. Water flows through the inner tube as the HTF to transfer thermal energy with the HNPCM during melting and solidification process. The thermophysical properties of the pure PCM and the nanoparticles used in the present study are presented in Table 1. For an equivalent quantity of the TiO_2–CuO hybrid nanoparticles, five

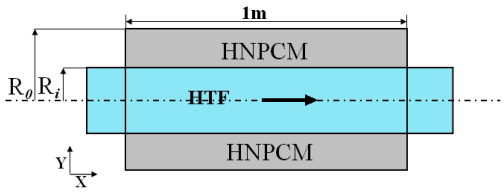

Fig. 1. Schematic diagram of the numerical TES system

Table 1. Thermo-physical properties of PCM [22], water [23], nanoparticles TiO_2 [24] and CuO [24]

Propriety	Paraffin	HTF (water)	Nanoparticles	
			TiO_2	CuO
Density (kg m^{-3})	778	977.36	4250	6460
Specific heat capacity (J kg^{-1} K^{-1})	2100	4066.8	686	536
Thermal conductivity (W m^{-1} K^{-1})	0.231	0.6627	8.954	10.042
Melting temperature (°C)	58–62	–	–	–
Latent heat (J kg^{-1})	189470	–	–	–
Viscosity (mPa s)	9.27	–	–	–
Dilatation coefficient (1/K)	0.0006	–	–	–

mass concentrations of 0%, 0.25%, 0.5%, 0.75% and 1 mass% were used in this study as shown in Table 2. The computations were performed for the charging and the discharging processes [23].

Table 2. Thermophysical properties of hybrid NanoPCM for each fraction

TiO_2–CuO					
Total fraction	0%	0.25%	0.5%	0.75%	1%
Density (kg m^{-3})	778	789.48	800.95	812.4	823.83
Heat capacity (J $kg^{-1}K^{-1}$)	2100	2074.41	2049.6	2025.51	2002.13
Thermal conductivity (W $m^{-1}K^{-1}$)	0.231	0.265	0.298	0.322	0.345
Viscosity (mPa s)	0.00927	0.00936	0.00947	0.00962	0.00984
Thermal expansion coefficient (1/K)	0.0006	0.00059	0.00058	0.00057	0.00056
Latent heat (J kg^{-1})	197620	196220	194680	192340	190060

3. Governing equations

The following assumptions are taken into account to conduct all the numerical simulations of the charging and discharging process of the HNPCM in the LHTES unit.

- The flow in the HTF and the liquid phase of the HNPCM inside the container is laminar, incompressible and Newtonian.
- The thermophysical properties, except the density, are assumed to be constant across temperature.
- The Boussinesq approximation is adopted to take into account the density variation.
- Volumetric expansion or contraction of samples associated with phase transition in the shell container is neglected.
- The HNPCM is homogeneous and isotropic.
- The external shell wall container is considered perfectly insulated, and the shell material is not taken into account in the computational domain.
- Due to the higher thermal conductivity relative to the copper tube, the thickness of tubes is neglected, and inlet temperature variations of HTF are also ignored.
- The continuity

$$\frac{\partial}{\partial x_i}(\rho u_i) = 0. \tag{1}$$

- The momentum

$$\frac{\partial \vec{V}}{\partial t} + \vec{V} \cdot \nabla \vec{V} = \frac{1}{\rho}\left(-\nabla P + \mu \nabla^2 \vec{V} + \rho \beta \vec{g}\,(T - T_0)\right) + \vec{S}. \tag{2}$$

- The energy

$$\frac{\partial H}{\partial t} + \nabla \cdot \left(\vec{V}\, H\right) = \nabla \left(\frac{k}{\rho C_p} \nabla h\right). \tag{3}$$

- The total volumetric enthalpy H is calculated by:

$$H = h + \Delta H, \tag{4}$$

$$\Delta H = \gamma L, \tag{5}$$

$$h = h_0 + \int_{T_0}^{T} C_p \, \mathrm{d}T, \tag{6}$$

where ΔH is the latent heat of the material and h is the sensible heat of PCM, h_0 is the PCM sensible enthalpy at the reference temperature T_0, γ refers to the liquid fraction that indicates the fraction of a cell volume in the liquid form and is associated with each cell in the domain as expressed by Eq. (7):

$$\gamma = \begin{cases} 0 & T < T_s\,, \\ \dfrac{T - T_s}{T_l - T_s} & T_s < T < T_l\,, \\ 1 & T > T_l\,. \end{cases} \tag{7}$$

The Boussinesq approximation was adopted to calculate the change in PCM density as a function of temperature in the liquid, given by:

$$\rho = \rho_0 \left[1 - \beta \left(T - T_0\right)\right] \tag{8}$$

and the relationship between the buoyancy forces in the momentum equation is given by:

$$-\rho g = \rho_0 g \left[\beta \left(T - T_m\right) - 1\right], \tag{9}$$

where ρ_0 is the reference density at the melting temperature T_m and β is the thermal expansion.

3.1. Thermal performance index

The total energy stored by the HNPCM during the charging process is defined by:

$$H_{\text{total}} = \int_{T_0}^{T_{\text{inlet}}} m c_p \, \mathrm{d}T + m\Delta H, \tag{10}$$

where T_{inlet} represents the inlet temperature of the HTF, m is the effective mass of the HNPCM, and ΔH is defined by Eq. (5).

The instantaneous stored energy of the HNPCM is defined by [19]:

$$H(t) = \int_{T_0}^{T_{\mathrm{HNPCM}}} mc_p \,\mathrm{d}T + m\gamma L. \tag{11}$$

We can use the dimensionless form of $H(t)$ dividing it by the maximum value H_{total} using (Eq. (10)), i.e., $H(t)/H_{\mathrm{total}}$.

Also, we can define the rate of the stored energy (Eq. (11)) as follows:

$$\bar{Q} = H(t)/t_{ch}\,. \tag{12}$$

3.2. Thermophysical properties of hybrid nano-PCM

Generally, to determine the nanofluid thermophysical properties, almost all of the literature studies have used the classical models of Maxwell [25]. However, a hybrid nanofluid lacks adequate models to define its properties. In fact, there is a model proposed by Ghadikolaei et al. [26] based on the classical ones. The mass concentration ϕ for the two different types of nanoparticles (TiO_2 and CuO) dispersed in the PCM is calculated from Eq. (10) and the other thermal properties are calculated according to the equations shown in Table 3.

$$\phi = \phi_{\mathrm{TiO_2}} + \phi_{\mathrm{CuO}}\,. \tag{13}$$

A comparison between the experimental results of Harikrishnan et al. [22] and the values predicted by classical models (Eq. (23) and Eq. (21)) of the HNPCM thermal conductivity and viscosity are illustrated in Fig. 2a and Fig. 2b, respectively. According to the figures, the applied equations (Eq. (23) and Eq. (21)) are

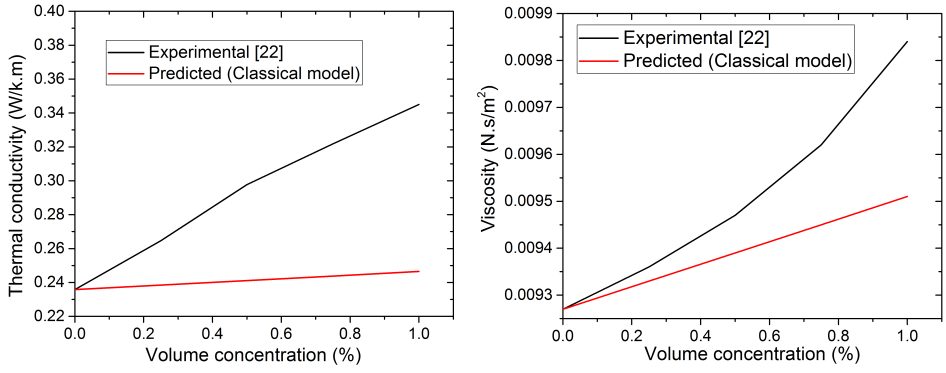

(a) thermal conductivity (b) dynamic viscosity

Fig. 2. Thermophysical properties of TiO_2–CuO/paraffin

Table 3. Thermophysical properties of hybrid NanoPCM [27]

NanoPCM		Hybrid NanoPCM	
$\rho_{\mathrm{nPCM}} = \rho_{\mathrm{PCM}}\left[(1-\phi)+\phi\left(\frac{\rho_s}{\rho_{\mathrm{PCM}}}\right)\right]$	(14)	$\rho_{\mathrm{HNPCM}} = \rho_{\mathrm{PCM}}(1-\phi_2)\left[(1-\phi_1)+\phi_1\left(\frac{\rho_{s_1}}{\rho_{\mathrm{PCM}}}\right)\right]+\phi_2\rho_{s_2}$	(19)
$\rho Cp_{\mathrm{nPCM}} = \rho Cp_{\mathrm{PCM}}\left[(1-\phi)+\phi\left(\frac{\rho Cp_s}{\rho Cp_{\mathrm{PCM}}}\right)\right]$	(15)	$\rho Cp_{\mathrm{HNPCM}} = \rho Cp_{\mathrm{PCM}}(1-\phi_2)\left[(1-\phi_1)+\phi_1\left(\frac{\rho Cp_{s_1}}{\rho Cp_{\mathrm{PCM}}}\right)\right]+\phi_2\rho Cp_{s_2}$	(20)
$\mu_{\mathrm{nPCM}} = \frac{\mu_{\mathrm{PCM}}}{(1-\phi)^{2.5}}$	(16)	$\mu_{\mathrm{HNPCM}} = \frac{\mu_{\mathrm{PCM}}}{(1-\phi_1)^{2.5}(1-\phi_2)^{2.5}}$	(21)
$\rho L_{f_{b\mathrm{PCM}}} = \rho L_{f_{b\mathrm{PCM}}}(1-\phi)$	(17)	$\rho L_{f_{\mathrm{HNPCM}}} = \rho L_{f_{bPCM}}(1-\phi_2)(1-\phi_1)$	(22)
$\frac{k_{\mathrm{nPCM}}}{k_{\mathrm{PCM}}} = \frac{k_s+(S-1)k_{\mathrm{PCM}}-(S-1)\phi\,(k_{\mathrm{PCM}}-k_s)}{k_s+(S-1)k_{\mathrm{PCM}}+\phi\,(k_{\mathrm{PCM}}-k_s)}$	(18)	$\frac{k_{\mathrm{HNPCM}}}{k_{\mathrm{bPCM}}} = \frac{k_{s_2}+(S-1)k_{\mathrm{bPCM}}-(S-1)\phi_2\,(k_{\mathrm{bPCM}}-k_{s_2})}{k_{s_2}+(S-1)k_{\mathrm{bPCM}}+\phi_2\,(k_{bPCM}-k_{s_2})}$ where $\frac{k_{\mathrm{bPCM}}}{k_{\mathrm{PCM}}} = \frac{k_{s_1}+(S-1)k_{\mathrm{PCM}}-(S-1)\phi_1\,(k_{\mathrm{PCM}}-k_{s_1})}{k_{s_1}+(S-1)k_{\mathrm{PCM}}+\phi_1\,(k_{\mathrm{PCM}}-k_{s_1})}$	(23)

acceptable only for a very low mass concentration of hybrid nanoparticles, while very large differences are observed for the high mass concentrations. Therefore, we can conclude that these classical models cannot estimate the hybrid thermophysical properties of the HNPCM with good precision. This makes it difficult to have a clear idea of the hybrid nanoparticles' influence on pure PCM. Accordingly, the thermal conductivity and viscosity of the HNPCM for all mass concentrations are taken from the measured experimental data of Harikrishnan et al. [22] for the present numerical computations.

4. Numerical method and validation

4.1. Numerical method

A 2D implicit finite volume method was used to solve the governing equations in section 3.1 for the heat transfer conjugated with the solid-liquid phase change process. The governing equations are solved by using the commercial code Ansys Fluent. The phase change phenomena were modelled by the enthalpy-porosity formulation [28]. In this method, the solid-liquid interface is modelled as a porous medium. The liquid fraction varies smoothly across this porous, the so-called mushy zone, where the porosity takes the values of 0 and 1 in the liquid and the solid phases, respectively. The mushy zone is modelled via the phase fractions incorporated in the source terms in the governing equations to account for the phase change phenomena.

The pressure-velocity coupling was taken into account by using the SIMPLE algorithm [29], whereas the Quick scheme was adopted for convective discrimination, and the PRESTO scheme was selected for pressure correction. Besides, the Boussineq approximation was adopted to take into account the change in density of the PCM in the liquid phase as a function of temperature, Eq. (7). Further, the convergence criteria of 10^{-6} for the momentum and continuity equations and 10^{-8} for the energy equation were taken.

4.1.1. Time step and grid independency tests

The grid size is very important for the accuracy of results and for saving the computational time. To determine the adequate grid size, a mesh independency test was performed. The study has been conducted using paraffin as the PCM, the HTF enters at 70°C with a flow rate of 0.017 kg/s. Three meshes of 13250, 17250 and 20250 grid resolutions are tested for the PCM liquid fraction for 0.1 s of time step. As can be seen in Fig. 3b, it is clear that the fixed grid resolution of 20250 is more adequate for the calculation. Finally, we adopted a time step of 0.1 s and the 20250 grid resolution to meet the accuracy and the convergence criteria for all simulations.

In addition, three time steps of 0.05 s, 0.1 s and 0.5 s have been tested to estimate the optimum for the fixed 20250 (135 × 150) grid resolution, as shown in Fig. 3a. The average PCM temperature evolutions for the time steps of 0.1 s and 0.05 s are almost identical. So, we have found that 0.1 s is an adequate value. The convergence has been confirmed at each time step, with the convergence criterion of 10^{-6} for all variables except the energy equation, where we took 10^{-8}.

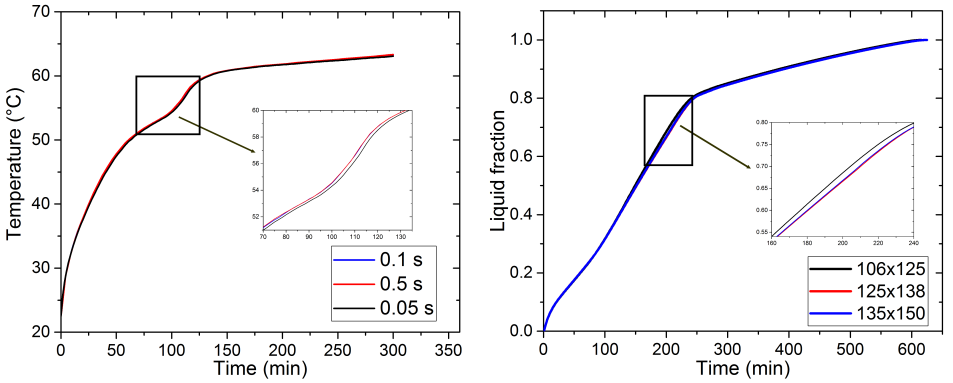

(a) average PCM temperature of different time steps

(b) liquid fraction grid resolution

Fig. 3. Time step and mesh size independency tests

4.1.2. Initial and boundary conditions

For the charging cycle, the initial temperature of the whole system is $T_0 = 25°C$. The HTF temperature is set to $T_{HTF} = 70°C$ with a flow rate of 0.017 kg/s. Besides, for the discharging cycle, only the HTF temperature must be lower than the HNPCM solidus temperature (45°C) to assure the complete solidification. Therefore, it is set to 25°C to recover the heat released by the HNPCM. The shell is assumed to be adiabatic, and the interfaces between the HNPCM and the HTF are set to be the coupled thermal boundaries (conjugate heat transfer).

4.2. Validation

The present model has been validated successfully with numerical and experimental data of Hosseini et al. [21]. Our validation has been performed with the same initial and boundary conditions, material properties and geometry as those of [21]. The total temperature of PCM for the charging process has been used for the validation. Fig. 4 shows the comparison between our predicted results and the experimental and numerical ones. According to Fig. 4, a good agreement was obtained. Therefore, it can be concluded that the present numerical model could be acceptable to predict the behavior of the PCM during the charging and the discharging process. Beside, in the previous study [30] we compared the outlet HTF

temperature for charging and discharging phases with the experimental results of Kibria et al. [31], Fig. 5a and Fig. 5b. It can be noticed that during charging and discharging cycles in both experiments the transient temperature curves are in good agreement.

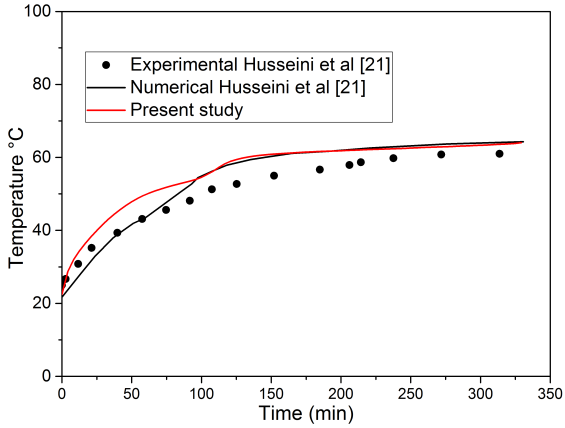

Fig. 4. Comparison of the average PCM temperatures for the charging process between numerical and experimental results of [21] and the present study

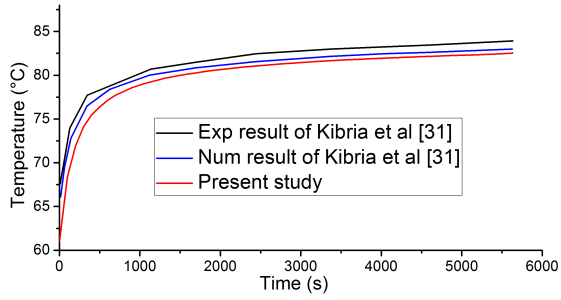

(a) for the charging

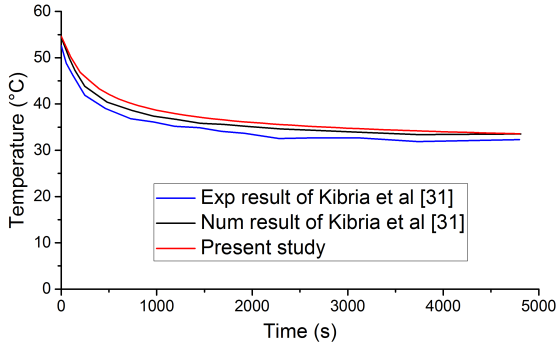

(b) for discharging

Fig. 5. Comparison of outlet temperature between numerical and experimental results of [31] and the authors' previous study [30]

5. Results and discussion

5.1. Charging/melting process

The effect of dispersed hybrid nanoparticles in the PCM samples from 0 to 1 wt% in the range of 0.25 wt% on the melting process is presented in Fig. 6. As we can see, the melting time decreased by 12%, 20%, 23.5% and 27.3%, respectively. This is due to the hybrid nano-improvement which enhances the effective thermal conductivity of the PCM. Furthermore, the hybrid nanoparticles accelerate the sensible heating process due to the PCMs high thermal conductivity, even though the HNPCM thermal conductivity increased by about 50% from 0.231 for pure PCM to 0.345 W/m K for 1 wt% of hybrid nanoparticles. The melting rate did not accelerate as fast as we expected because of the increase in viscosity by about 6.14% compared to the pure PCM. This effect slows down the motion of molten HNPCM, then reduces the natural convection effect. Therefore, the thermal conductivity improvement can not only accelerate the phase change but also increases its low dynamic viscosity.

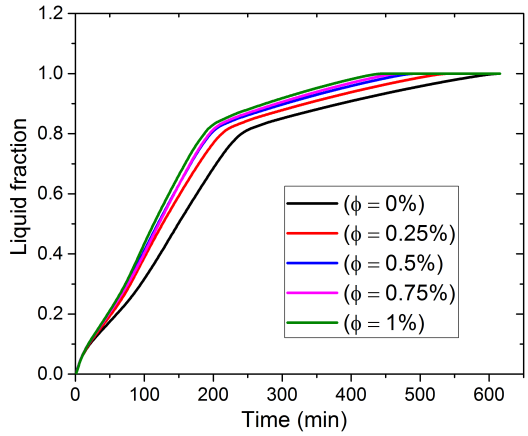

Fig. 6. Liquid fraction of the HNPCM samples during charging process

The complete melting temperature of all HNPCM samples versus time are shown in Fig. 7. We can divide this graphic into three ranges.

- The solid sensible heating range: We can see that the average temperature increases rapidly in all the cases because of domination of the conduction heat transfer in the solid phase.
- The phase change range: In this phase, it is clear that the average temperature in the HNPCM does not differ much between all the cases. When the thermal conductivity increases, the phase change rate increases slightly because of slow motion of the liquid HNPCM. There, the viscosity rises by about

1%, 2.16%, 3.77%, and 6.15% compared with the pure PCM value (υ_{PCM} 0.00927 kg/m^{2}s) for all the HNPCM samples, respectively. Besides, the dynamic viscosity increase affects the role of natural convection in the liquid HNPCM.

- The liquid sensible heating range: When the HNPCM has completely melted, its temperature becomes almost constant near the HTF inlet temperature of 343K. Also, as shown in Fig. 7, the melting time decreases from 616 min in pure PCM to 448 min for the HNPCM with 1 wt% sample. That is a decrease by about 27.3%, which is due to the high nano-hybrid optimization performance.

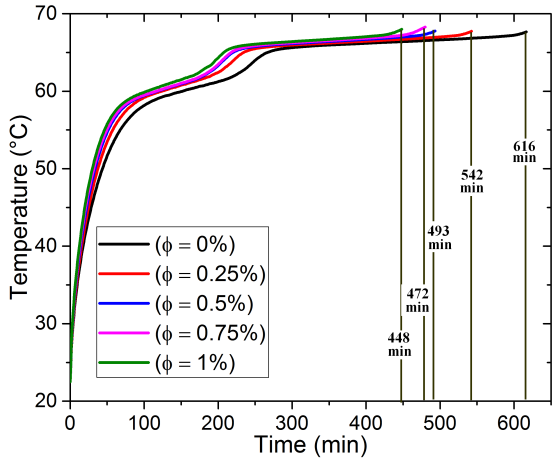

Fig. 7. The total average temperature of the HNPCM samples during the complete melting (charging process)

From the above equations, one can notice that as the mass concentration of hybrid nanoparticles increases, the density and the thermal conductivity increase, while the latent heat and the specific heat capacity decrease. As a result, the total thermal energy stored by the system decreases. The dimensionless stored energy of 0%, 0.25%, 0.5%, 0.75%, and 1% in HNPCM samples for the complete melting is presented in Fig. 8. As the time elapses, the $H(t)/H_{\text{total}}$ increases almost linearly due to the sensible heating of the solid HNPCM. When the liquid fraction increases slightly with time due to the phase change, the evolution of $H(t)/H_{\text{total}}$ becomes non-linear. At the end of the charging process, the $H(t)/H_{\text{total}}$ reaches the steady state taking the value of 1 when the HNPCM average temperature approaches the HTF inlet temperature.

The increment of the hybrid nanoparticles mass concentration decreases the HNPCM latent heat capacity. That decreases the effective storage mass of the pure PCM replaced by a HNCPM with hybrid nanoparticles. As shown in Fig. 9, the

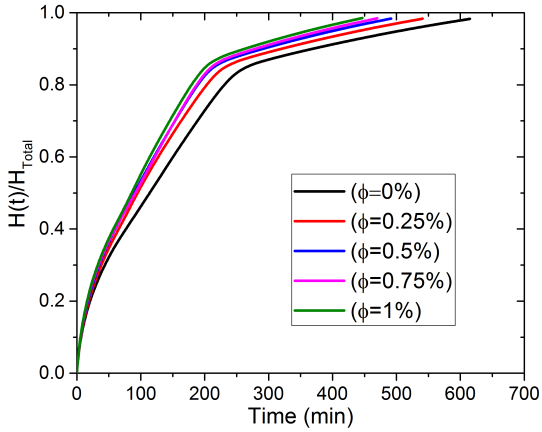

Fig. 8. The nanoparticles mass concentration effect on the dimensionless stored energy time evolution of the HNPCM samples during the complete charging process

stored energy decreases from 286 kJ/kg for the pure PCM to 275 kJ/kg for the HNPCM with ϕ = 1% which means a decrease by about 3.86%.

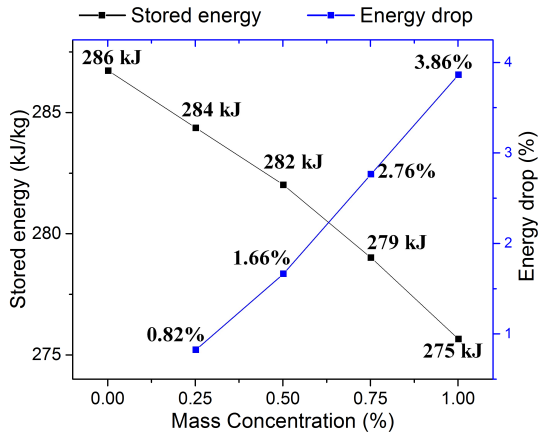

Fig. 9. The HNPCM stored energy and its percentage drop

The completely melting time of HNPCM samples is illustrated by Fig. 10. We can see that the melting time reduces by 12.04%, 19.9%, 23.55%, and 27.33% when the mass concentration of hybrid nanoparticles increases by 0.25, 0.5, 0.75, and 1 wt%, respectively. This is because of the thermal conductivity improvement which rises from 0.231 W/(m K) for the pure PCM to 0.345 W/(m K)pfor the HNPCM (ϕ = 1%). Besides, the effective heat transfer surface is significantly improved, which can generate a higher charging rate.

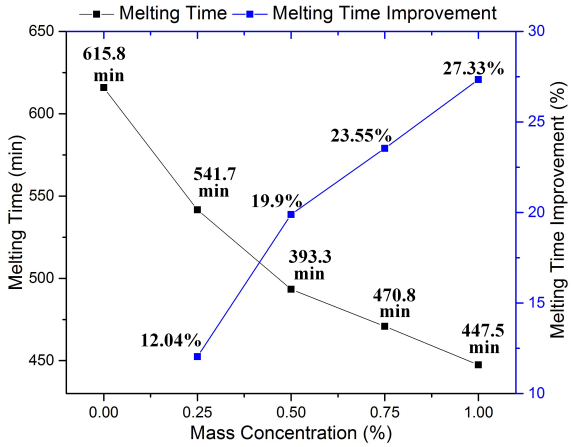

Fig. 10. The HNPCM melting time and its improvement

5.1.1. Thermal behavior of hybrid nano-PCM

The melting of HNPCM at a constant inlet temperature of 343 K is presented in Fig. 11. At the earlier stage of melting (Fig. 11(a)), the cold HNPCM absorbs thermal energy from the hot HTF and starts to melt. The fraction of liquid HNPCM at this time is almost equal to about 8% at 15 min, where the conduction drives the heat transfer. As the time elapsed, the HNPCM absorbs more energy and the liquid quantity increases in different amounts because of the different thermal conductivity improvement. When the volume of liquefied HNPCM increases, the convection dominates the heat transfer. As we can see in Fig. 11(b, c), the quantity of melted HNPCM is greater in the inlet, then it becomes smaller near the outlet. This is because of the drop in the HTF temperature caused by the HNPCM. Also,

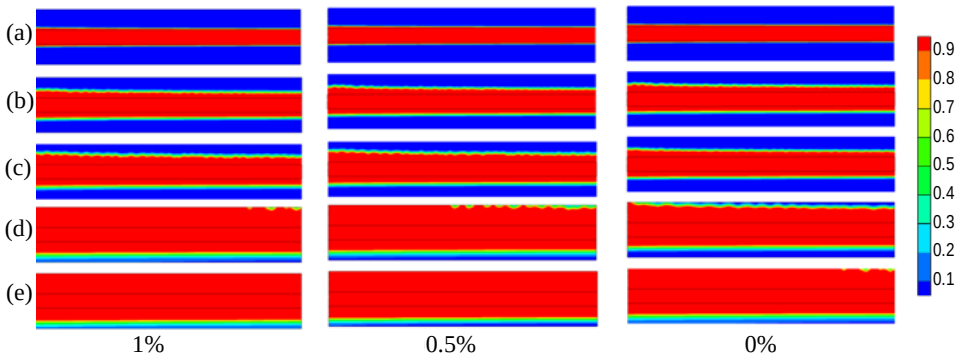

Fig. 11. Liquid fraction contours of HNPCM sample with 0%, 0.5%, and 1% mass concentration within different time ranges and a constant inlet temperature of 343 K: (a) 15 min, (b) 75 min, (c) 100 min, (d) 200 min and (e) 250 min

the solid HNPCM melts faster at the top of the TES unit than at the bottom, which is caused by the flux of molten convective liquid that moves up and down accelerating the solid to liquid transition. However, at the lower part of Fig. 11(d, e), one can see stratification layers of the HNPCM with different temperatures, because there the conduction drives the heat transfer. Therefore, the solid HNPCM at this region presents a greater thermal resistance increasing its melting time, which becomes longer compared with the that at the top region.

5.2. Discharging/solidification phase

The liquid fraction evolution with time during the discharging phase is shown in Fig. 12. Compared with the charging process, the discharging time for all cases decreases considerably because of the large difference between the inlet HTF and the solidification temperature of the HNPCM. These lead to an earlier solidification process which reduced the solidification time. In fact, the time of energy release from the hot liquid HNPCM to water is reduced by 30.52% for the case of 1% of hybrid nanoparticles.

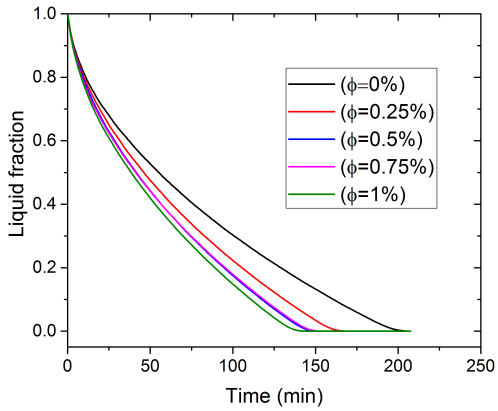

Fig. 12. Liquid fraction of the HNPCM samples during discharging process

The average HNPCM temperature for the discharging process is presented in Fig. 13. It is clear that the solidification time is small compared to the charging phase, as it is decreased by about 18.47%, 26.91%, 27.71%, and 30.52% for 0.25%, 0.5%, 0.75%, and 1 mass%, respectively. As we explained above, the high difference between the mean melting temperature of the HNPCM and that of the inlet HTF speeds up the sensible removing heat process.

The complete solidification time and its percentage improvement for all the samples is presented in Fig. 14. We can see from this figure that the solidification time drops from 207.5 min for the pure PCM case to 169, 152, 150 and 144 min for the 0.25, 0.5, 0.75 and 1 wt% HNPCM samples respectively. Therefore, the

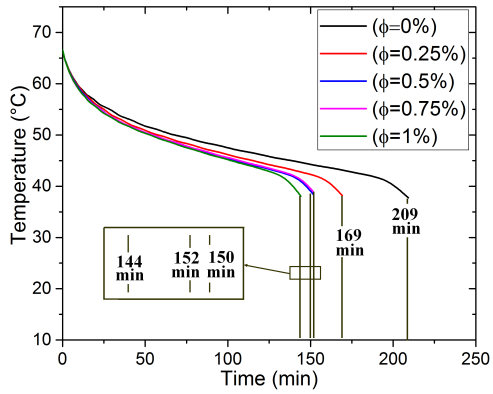

Fig. 13. The total average temperature of the HNPCM samples during discharging process

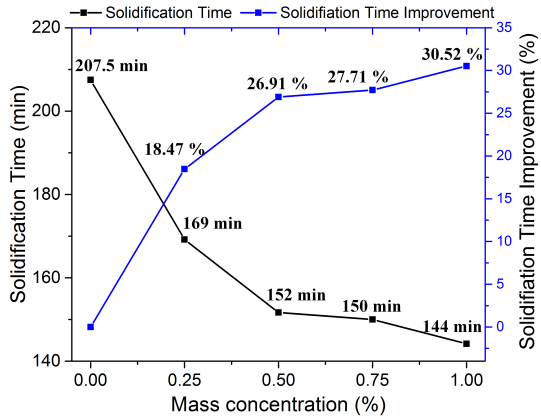

Fig. 14. The HNPCM solidification time and its improvement

solidification rate improves by 18, 47%, 26, 91%, 27.71%, and 30.52%, respectively. This significant improvement is due to the increase in thermal conductivity and viscosity of the HNPCM. In fact, the viscosity increase slows down the liquid HNPCM motion which reduces the natural convection effect. Hence, it allows for the domination of the conduction, which becomes more effective by increasing the thermal conductivity. Therefore, the discharging process requires a shorter time compared with the pure PCM case.

The solidification process for different time and mass concentrations is presented in Fig. 15. In this phase, the cold water enters with a temperature of 298 K and 0.017 kg/s flow rate to recover the heat energy released from the hot liquid

HNPCM. Firstly, the layer near the central tube wall of the unit starts to solidify because of the low HTF temperature. There, the solid fraction at the time of 10 min ranges from 19% to 22.7% for 0% to 1% of hybrid nanoparticles mass concentration. At the time of 60 min, it becomes clear (Fig. 15(b)) that the solid fraction increases rapidly. This is because of the high difference in temperature between the cold inlet HTF and the solidification temperature of the HNPCM, which makes the discharging process faster than the melting. The thermal conductivity improvement accelerates releasing the heat from the liquid hot HNPCM to the HTF by conduction. Furthermore, at the times of 100 and 140 min, the solid fraction increases naturally until the complete solidification. Therefore, it can be found that the discharging process is enhanced by 18.47%, 26.91%, 27.71% and 30.52%, for the 0.25, 0.5, 0.75 and 1 wt% HNPCM samples, respectively.

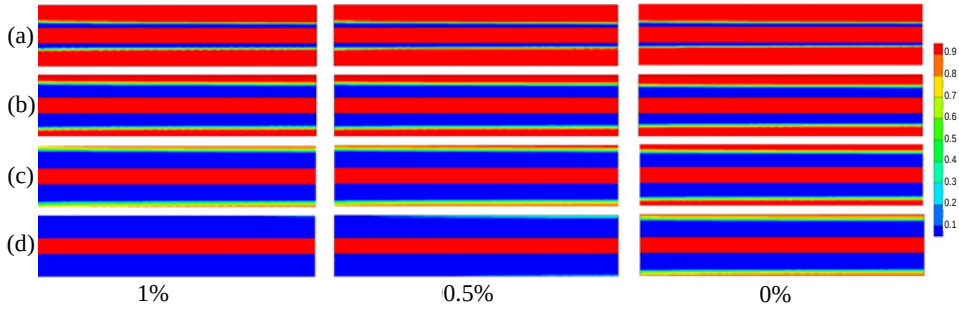

Fig. 15. Liquid fraction contours of HNPCM sample with 0%, 0.5%, and 1% mass concentration at different time ranges at constant inlet temperature of 295 K: (a) 10 min, (b) 60 min, (c) 100 min and (d) 140 min

6. Conclusion

The improvement of the shell and tube LHESS properties due to the introduction of hybrid nano-particles (50%–50% of TiO_2–CuO) was numerically studied in this paper. The numerical simulation has been conducted to evaluate the thermal performance enhancement in terms of both charging (melting) and discharging (solidification) processes in the TES unit filled by the PCM in which the particles of TiO_2–CuO (50%–50%) were dispersed as the hybrid nanoparticles to improve its thermal performance. The numerical model has been validated successfully by comparing the average melting PCM temperature with experimental studies, and a good agreement has been obtained. Also, the mathematical formulations have been used to estimate the thermophysical properties of the HNPCM.

Based on this study, the following conclusions are obtained:

- Mathematical formulations used in the literature to estimate the thermal properties of the hybrid-nano PCM cannot predict the real ones with a good precision. Especially, it pertains to the thermal conductivity and dynamic

viscosity parameters which have a strong effect on the thermal behavior of the PCM for this application. Accordingly, it is suitable to use realistic properties in such cases.

- The stored energy decreases due to the increase in concentration of the hybrid nanoparticles, which reduces the effective storage mass of the PCM. Therefore, the energy decreases by about 3.86% for $\phi = 1$ wt%.
- The HNPCM dynamic viscosity is increased when the hybrid nanoparticles' mass concentration is increased. Hence, the phase change rate is reduced due to the slower motion of the liquid HNPCM, which impedes the natural convection effect. Consequently, the melting time does not decrease as quickly as we would expect when the thermal conductivity of the HNPCM increases.
- For the melting process, the conduction dominates in the heat transfer at the first stage. Then, when the liquid HNPCM mass increases with time, the convection drives the heat transfer but not as effectively as we could expect due to the increase of the dynamic viscosity. However, for the discharging process, the conduction drives the heat transfer for the whole time required for the solidification.
- In the charging process, when the HNPCM mass fraction increases by 0.25, 0.5, 0.75, and 1 wt% the melting average time is shortened by 3.45%, 10.34%, 16.1% and 28.73%, respectively. At the same time, the stored energy is reduced by 0.83%, 1.67%, 2.83% and 3.88%, respectively.
- In the discharging process, the registered time for complete solidification was reduced by 18, 47%, 26, 91%, 27.71%, and 30.52%, respectively. Besides, it was smaller than the time required for melting because of the high difference between the inlet HTF temperature and that of solidification of the HNPCM. Therefore, it is appropriate to use a PCM with a melting temperature near the inlet HTF to control the discharging time.

Further studies will focus on the evaluation of several other metal-oxide couples in order to determine the optimum thermal properties needed to obtain the best performance of the TES.

References

[1] L.F. Cabeza, A. Castell, C. Barreneche, A. de Gracia, and A. Fernández. Materials used as PCM in thermal energy storage in buildings: A review. *Renewable and Sustainable Energy Reviews*, 15(3):1675–1695, 2011. doi: 10.1016/j.rser.2010.11.018.

[2] K. Nedjem, M. Teggar, K.A.R. Ismail, and D. Nehari. Numerical investigation of charging and discharging processes of a shell and tube nano-enhanced latent thermal storage unit. *Journal of Thermal Science and Engineering Applications*, 12(2):021021, 2020. doi: 10.1115/1.4046062.

[3] K. Hosseinzadeh, M.A. Efrani Moghaddam, A. Asadi, A.R. Mogharrebi, and D.D. Ganji. Effect of internal fins along with hybrid nano-particles on solid process in star shape triplex latent heat thermal energy storage system by numerical simulation. *Renewable Energy*, 154:497–507, 2020. doi: 10.1016/j.renene.2020.03.054.

[4] M.M. Joybari, S. Seddegh, X. Wang, and F. Haghighat. Experimental investigation of multiple tube heat transfer enhancement in a vertical cylindrical latent heat thermal energy storage system. *Renewable Energy* 140:234–244, 2019. doi: 10.1016/j.renene.2019.03.037.

[5] A.A. Al-Abidi, S. Mat, K. Sopian, M.Y. Sulaiman, and A.T. Mohammad. Internal and external fin heat transfer enhancement technique for latent heat thermal energy storage in triplex tube heat exchangers. *Applied Thermal Engineering*, 53(1):147–156, 2013. doi: 10.1016/j.applthermaleng.2013.01.011.

[6] X. Yang, Z. Lu, Q. Bai, Q. Zhang, L. Jin, and J. Yan. Thermal performance of a shell-and-tube latent heat thermal energy storage unit: Role of annular fins. *Applied Energy*, 202:558–570, 2017. doi: 10.1016/j.apenergy.2017.05.007.

[7] C. Zhao, M. Opolot, M. Liu, F. Bruno, S. Mancin, and K. Hooman. Numerical study of melting performance enhancement for PCM in an annular enclosure with internal-external fins and metal foams. *International Journal of Heat and Mass Transfer*, 150:119348, 2020. doi: 10.1016/j.ijheatmasstransfer.2020.119348.

[8] M. Longeon, A. Soupart, J.-F. Fourmigué, A. Bruch, and P. Marty. Experimental and numerical study of annular PCM storage in the presence of natural convection. *Applied Energy*, 112:175–184, 2013. doi: 10.1016/j.apenergy.2013.06.007.

[9] S. Seddegh, S.S.M. Tehrani, X. Wang, F. Cao, and R.A. Taylor. Comparison of heat transfer between cylindrical and conical vertical shell-and-tube latent heat thermal energy storage systems. *Applied Thermal Engineering*, 130:1349–1362, 2018. doi: 10.1016/j.applthermaleng.2017.11.130.

[10] I. Al Siyabi, S. Khanna, T. Mallick, and S. Sundaram. An experimental and numerical study on the effect of inclination angle of phase change materials thermal energy storage system. *Journal of Energy Storage*, 23:57–68, 2019. doi: 10.1016/j.est.2019.03.010.

[11] S. Sebti, S. Khalilarya, I. Mirzaee, S. Hosseinizadeh, S. Kashani, and M. Abdollahzadeh. A numerical investigation of solidification in horizontal concentric annuli filled with nano-enhanced phase change material (NEPCM). *World Applied Sciences Journal*, 13(1):9–15, 2011.

[12] N. Dhaidan, J. Khodadadi, T.A. Al-Hattab, and S. Al-Mashat. Experimental and numerical investigation of melting of NePCM inside an annular container under a constant heat flux including the effect of eccentricity. *International Journal of Heat and Mass Transfer*, 67:455–468, 2013. doi: 10.1016/j.ijheatmasstransfer.2013.08.002.

[13] Q. Ren, F. Meng, and P. Guo. A comparative study of PCM melting process in a heat pipe-assisted LHTES unit enhanced with nanoparticles and metal foams by immersed boundary-lattice Boltzmann method at pore-scale. *International Journal of Heat and Mass Transfer*, 121:1214–1228, 2018. doi: 10.1016/j.ijheatmasstransfer.2018.01.046.

[14] C. Nie, J. Liu, and S. Deng. Effect of geometric parameter and nanoparticles on PCM melting in a vertical shell-tube system. *Applied Thermal Engineering*, 184:116290, 2020. doi: 10.1016/j.applthermaleng.2020.116290.

[15] M. Gorzin, M.J. Hosseini, M. Rahimi, and R. Bahrampoury. Nano-enhancement of phase change material in a shell and multi-PCM-tube heat exchanger. *Journal of Energy Storage*, 22:88–97, 2019. doi: 10.1016/j.est.2018.12.023.

[16] M. Khatibi, R. Nemati-Farouji, A. Taheri, A. Kazemian, T. Ma, and H. Niazmand. Optimization and performance investigation of the solidification behavior of nano-enhanced phase change materials in triplex-tube and shell-and-tube energy storage units. *Journal of Energy Storage*, 33:102055, 2020. doi: 10.1016/j.est.2020.102055.

[17] P. Manoj Kumar, K. Mylsamy, and P.T. Saravanakumar. Experimental investigations on thermal properties of nano-SiO_2/paraffin phase change material (PCM) for solar thermal energy storage applications. *Energy Sources, Part A: Recovery, Utilization, and Environmental Effects*, 42(19):2420–2433, 2020. doi: 10.1080/15567036.2019.1607942.

[18] P. Manoj Kumar, K. Mylsamy, K. Alagar, and K. Sudhakar. Investigations on an evacuated tube solar water heater using hybrid-nano based organic phase change material. *International Journal of Green Energy*, 17(13):872–883, 2020. doi: 10.1080/15435075.2020.1809426.

[19] S. Ebadi, S.H. Tasnim, A.A. Aliabadi, and S. Mahmud. Melting of nano-PCM inside a cylindrical thermal energy storage system: Numerical study with experimental verification. *Energy Conversion and Management*, 166:241–259, 2018. doi: 10.1016/j.enconman.2018.04.016.

[20] J.M. Mahdi and E.C. Nsofor. Solidification enhancement of PCM in a triplex-tube thermal energy storage system with nanoparticles and fins. *Applied Energy*, 211:975–986, 2018. doi: 10.1016/j.apenergy.2017.11.082.

[21] M.J. Hosseini, A.A. Ranjbar, K. Sedighi, and M. Rahimi. A combined experimental and computational study on the melting behavior of a medium temperature phase change storage material inside shell and tube heat exchanger. *International Communications in Heat and Mass Transfer*, 39(9):1416–1424, 2012. doi: 10.1016/j.icheatmasstransfer.2012.07.028.

[22] S. Harikrishnan, K. Deepak, and S. Kalaiselvam. Thermal energy storage behavior of composite using hybrid nanomaterials as PCM for solar heating systems. *Journal of Thermal Analysis and Calorimetry*, 115:1563–1571, 2014. doi: 10.1007/s10973-013-3472-x.

[23] ANSYS. Fluent. (2017), Copyright 2017 SAS IP, Inc.

[24] Z. Khan, Z.A. Khan, and P. Sewell. Heat transfer evaluation of metal oxides based nano-PCMs for latent heat storage system application. *International Journal of Heat and Mass Transfer*, 144:118619, 2019. doi: 10.1016/j.ijheatmasstransfer.2019.118619.

[25] J.C. Maxwell. *Electricity and Magnetism*. Clarendon Press, Oxford, 1873.

[26] S. Ghadikolaei, K. Hosseinzadeh, and D.D. Ganji. Investigation on three dimensional squeezing flow of mixture base fluid (ethylene glycol-water) suspended by hybrid nanoparticle (Fe_3O_4-Ag) dependent on shape factor. *Journal of Molecular Liquids*, 262:376–388, 2018. doi: 10.1016/j.molliq.2018.04.094.

[27] S.S. Ghadikolaei, M. Yassari, H. Sadeghi, K. Hosseinzadeh, and D.D. Ganji. Investigation on thermophysical properties of TiO_2–Cu/H_2O hybrid nanofluid transport dependent on shape factor in MHD stagnation point flow. *Powder Technology*, 322:428–438, 2017. doi: 10.1016/j.powtec.2017.09.006.

[28] A.D. Brent, V.R. Voller, and K. Reid. Enthalpy-porosity technique for modeling convection-diffusion phase change: application to the melting of a pure metal. *Numerical Heat Transfer*, 13(3):297–318, 1988. doi: 10.1080/10407788808913615.

[29] S.V. Patankar. *Numerical Heat Transfer and Fluid Flow*. CRC Press, 1980.

[30] M.L. Benlekkam, D. Nehari, and N. Cheriet. Numerical investigation of latent heat thermal energy storage system. *Recueil de Mécanique*, 3:229-235, 2018. doi: 10.5281/zenodo.1490505.

[31] M.A. Kibria, M.R. Anisur, M.H. Mahfuz, R. Saidur, and I.H.S.C. Metselaar. Numerical and experimental investigation of heat transfer in a shell and tube thermal energy storage system. *International Communications in Heat and Mass Transfer*, 53:71–78, 2014. doi: 10.1016/j.icheatmasstransfer.2014.02.023.

[32] M.J. Hosseini, M. Rahimi, and R. Bahrampoury. Experimental and computational evolution of a shell and tube heat exchanger as a PCM thermal storage system. *International Communications in Heat and Mass Transfer*, 50:128–136, 2014. doi: 10.1016/j.icheatmasstransfer.2013.11.008.